

# Critical Decrease in the Level of Axon Guidance Receptor ROBO1 in Rod Synaptic Terminals Is Followed by Axon Retraction

Tatyana Appelbaum, Evelyn Santana, and Gustavo D. Aguirre

Department of Clinical Sciences & Advanced Medicine, School of Veterinary Medicine, University of Pennsylvania, Philadelphia, Pennsylvania, United States

Correspondence: Tatyana Appelbaum, School of Veterinary Medicine, University of Pennsylvania, 3900 Delancey Street, Philadelphia, PA 19104, USA; [tatyanak@upenn.edu](mailto:tatyanak@upenn.edu).

**Received:** October 8, 2019  
**Accepted:** December 14, 2019  
**Published:** March 16, 2020

Citation: Appelbaum T, Santana E, Aguirre GD. Critical decrease in the level of axon guidance receptor ROBO1 in rod synaptic terminals is followed by axon retraction. *Invest Ophthalmol Vis Sci.* 2020;61(3):11. <https://doi.org/10.1167/iovs.61.3.11>

**PURPOSE.** To define remodeling of photoreceptor synaptic terminals and second-order retinal neurons in canine X-linked progressive retinal atrophy 1 caused by a five-nucleotide deletion in the *RPGR* exon ORF15.

**METHODS.** Retinas of normal and mutant dogs were used for gene expression, Western blot, and immunohistochemistry. Cell-specific markers were used to examine disease-dependent retinal remodeling.

**RESULTS.** In mutant retinas, a number of rod axon terminals retract into the outer nuclear layer. This neuritic atrophy preceded significant loss of rods and was evident early in disease. Rod bipolar and horizontal cell processes were found to extend into the outer nuclear layer, where they seemed to form contacts with the spherules of rod photoreceptors. No ectopic rewiring was observed. Because cytoskeletal reorganization was previously shown to underlie photoreceptor axon retraction, we examined normal and mutant retinas for expression of axon guidance receptors ROBO1 and ROBO2, which are known to regulate actin cytoskeleton dynamics. We found that the overall expression of both *ROBO1* and *ROBO2* is retained at the same level in premature and fully developed normal retinas. However, analysis of predisease and early disease retinas identified markedly decreased levels of ROBO1 in rod spherules compared with controls. In contrast, no differences in ROBO1 signals were noted in cone pedicles in normal and mutant retinas, where ROBO1 levels remained similarly low.

**CONCLUSIONS.** Depletion of ROBO1 in rod synaptic terminals correlates with the remodeling of axonal and dendritic processes in the outer retina of dogs with X-linked progressive retinal atrophy 1 and may play a role in the retraction of rod axons.

**Keywords:** X-linked retinitis pigmentosa (XLRP), retinal remodeling, retinal degeneration, axon guidance receptors

**RP** is a heterogeneous group of inherited retinal degenerative diseases leading to photoreceptor (PR) cell death and vision loss.<sup>1</sup> Rod-cone dystrophy, the prevalent form of RP, is characterized by primary dysfunction and loss of rod PRs and associated with cones death at later stages as well as abnormalities in the adjacent RPE. Loss of PRs further triggers functional changes in second-order retinal neurons (bipolar and horizontal cells [HCs]) and third-order retinal neurons (amacrine and retinal ganglion cells), resulting in regressive remodeling of the inner retina.<sup>2-4</sup> Within RP groups, X-linked RP comprises some of the most severe forms of the disease, and account for 10% to 20% of all RP cases.<sup>5</sup> Of six disease loci mapped on the X-chromosome (<https://sph.uth.edu/retnet/disease.htm>) approximately 75% of X-linked RP cases map to the RP3 locus<sup>6,7</sup> that contains the disease causative RP GTPase regulator (*RPGR*) gene.<sup>8,9</sup>

The mechanism underlying *RPGR*-dependent X-linked RP pathogenesis remains poorly understood. There are two major isoforms of *RPGR* (*RPGR*<sup>1-19</sup> and *RPGR*<sup>orf15</sup>) that

are expressed in the retina.<sup>9,10</sup> *RPGR*<sup>orf15</sup> is predominantly expressed in PR sensory cilia and basal bodies<sup>11</sup> and plays a critical role in retinal function and viability, as multiple disease-causing mutations have been mapped to this isoform in humans, dogs, and mice.<sup>8,12,13</sup> To date, the X-linked progressive retinal atrophy (XLPRA) dog is the only known naturally occurring large animal model of *RPGR*<sup>orf15</sup>-XLRP.<sup>13</sup>

Two disease-causing mutations in exon ORF15 have been identified in canine *RPGR*.<sup>13</sup> One mutation is a five-nucleotide deletion (del1028-1032) that produces a premature stop codon that results in a C-terminal truncation of 230 residues and is causal for XLPRA1. The second mutation is a 2-bp deletion (del1084-1085) that induces a frameshift, resulting in an inclusion of 34 basic amino acids and truncation of the terminal 161 residues, and is causal for XLPRA2. XLPRA1-affected dogs have normal PR morphogenesis, after which progressive rod-cone degeneration develops in the peripheral retina, gradually advancing toward the optic disc.<sup>14</sup> The phenotype associated with XLPRA2 is very severe

and manifests during early retinal development.<sup>15</sup> Together, these canine models have been proven useful in exploring pathogenic mechanisms of XLPR and testing clinical therapeutic strategies.<sup>16–19</sup>

Retinal remodeling in XLPRA1 has not been thoroughly characterized to date, as has been the case for XLPRA2 and some other retinal diseases in dogs. In this study, we examined remodeling of PR synaptic terminals and second-order retinal neurons in XLPRA1 retinas. Disruption of these synaptic contacts contributes to impairment of visual circuits, and is the underlying basis of disease-associated neuronal remodeling, including rod neurite sprouting<sup>17,20</sup> and retraction of the axon terminals of rod PRs,<sup>3,21–24</sup> as well as the aberrant outgrowth of rod bipolar cell (RBC) dendrites and HC processes into the outer nuclear layer (ONL).<sup>3,22</sup>

A limited number of molecular players modulating rod PR axonal retraction have been identified. Prior studies showed that activation of the Ras homolog family member A (RHOA, a member of the RHO family of small GTPases) and downstream RHO kinase activity contributes to retraction of the axon terminals of rod PRs.<sup>21,23</sup> However, the upstream molecular events responsible for triggering RHOA activity remain uncertain. During the development of the nervous system, a number of axon guidance cues and receptors guide axon movement by regulating the activity of RHO GTPases. The consequent activation of RHO kinases impacts actin cytoskeleton dynamics.<sup>25–28</sup> Binding of Roundabout receptors (ROBO) to their cognate SLIT ligands play a critical role in axon guidance. Because ROBO can inactivate RHO GTPases, including RHOA,<sup>26–28</sup> we hypothesized that the SLIT/ROBO pathway may promote synaptic and axonal stability in rod PRs.

Such hypothesis can be well-supported by expression of axon guidance receptors ROBO in rod axons and synaptic terminals, but the presence of ROBO proteins in mammalian PRs is hitherto undescribed. Whereas SLIT/ROBO pathway is best known for mediating axon repulsion in the developing nervous system, including central nervous system/retina,<sup>26,28,29</sup> the input of SLIT/ROBO pathway into control of neural circuits in fully developed adult mammalian retina has yet to be examined. Besides, very little is known about expression patterns of ROBO in adult retina.<sup>30–32</sup> Because ROBO1 and ROBO2 had not been annotated in the dog genome, we carried out a detailed characterization of the *ROBO1/ROBO2* genes and corresponding proteins in adult dog retina. Furthermore, using confocal microscopy we evaluated the possible involvement of ROBO signaling in the disease-associated altered lamination patterns of rod PR, RBC, and HC neurites. Our data support the functional significance of axon guidance receptors ROBO1 and ROBO2 in the retina, with ROBO1 acting as an important determinant of the XLPRA1 phenotype.

## METHODS

### Ethics Statement

The research was conducted in full compliance and in accordance with the Association for Research in Vision and Ophthalmology (ARVO) Resolution on the Use of Animals in Ophthalmic and Vision Research. All the studies have been approved by the University of Pennsylvania Institutional Animal Care and Use Committee.

## Tissue Samples

The study used archival canine retinal samples from normal and XLPRA1 dogs (listed in Supplementary Table S1) that were primarily gathered for previously published studies.<sup>17–19</sup> Other archival tissues, collected and stored at the Retinal Disease Studies facility included frozen blood, retina, testis, brain, kidney, spleen, and liver, and they were used for DNA/RNA extraction. The sectioned mouse retina (1 month old) was a kind gift from Dr Helen Léger (School of Veterinary Medicine, University of Pennsylvania). The human retina (79 years old) was processed in Dr Joshua Dunaief's laboratory (School of Medicine, University of Pennsylvania) and was collected adhering to the principles of the Declaration of Helsinki. OCT-embedded retinas from rat (1.5 months old) and normal nonhuman primate (4.9 years old) used for immunohistochemistry, were archival samples left from previous laboratory projects.

## DNA/RNA Extraction, cDNA Synthesis, and 5'-RACE

Genomic DNA was isolated from blood using the QIAamp DNA kit (Qiagen, Hilden, Germany) following the manufacturer's directions. Total RNA was isolated from canine tissues using a modified TRIzol and single chloroform extraction protocol as previously described. First strand cDNA for real-time PCR was synthesized using the High Capacity RNA-to-cDNA kit (Applied Biosystems, Foster City, CA) following the manufacturer's recommendations. First strand cDNA for full length transcripts analysis was gained using ThermoScript RT-PCR System (Life Technologies, Carlsbad, CA). Using the gene-specific primers listed in Supplementary Table S2, 5'-RACE was performed with the RNA-ligase-mediated RACE system (Thermo Fisher Scientific, Rockford, IL), according to the manufacturer's recommendations and.

## Amplification of Long PCR Fragments

Long-range PCR was performed using GoTaq Long PCR Master Mix (Promega, Madison, WI). Corresponding primers sequences are listed in Supplementary Table S2. All novel transcript data generated in this study have been deposited to the National Center for Biotechnology Information/GenBank database and accession numbers are listed in Supplementary Table S2.

## Relative Quantification (ddCt) Assay

Gene expression of *ROBO1* and *ROBO2* was determined by quantitative RT-PCR in age-matched 3-, 5-, 7-, and 16-week-old normal and 16-week-old XLPRA1-affected retinas. Each group analyzed included three animals. Real-time PCR was performed in a total volume of 25  $\mu$ L in 96-well microwell plates on the Applied Biosystems 7500 Real-Time PCR System. All PCRs were performed in triplicate using cDNA generated from 20 ng DNAase-treated RNA. The SYBR green platform was used for gene expression analysis using a primer concentration of 0.2  $\mu$ M. The TATA-box binding protein (*TBP*) gene expression level was used to normalize the cDNA templates using previously described primers.<sup>18</sup> Other primers used are listed in Supplementary Table S2. Amplification data were analyzed with the 7500 Software version 2.0.1 (Applied Biosystems). The unpaired *t*-test was used for statistical analysis. Genes with a *P* value of less

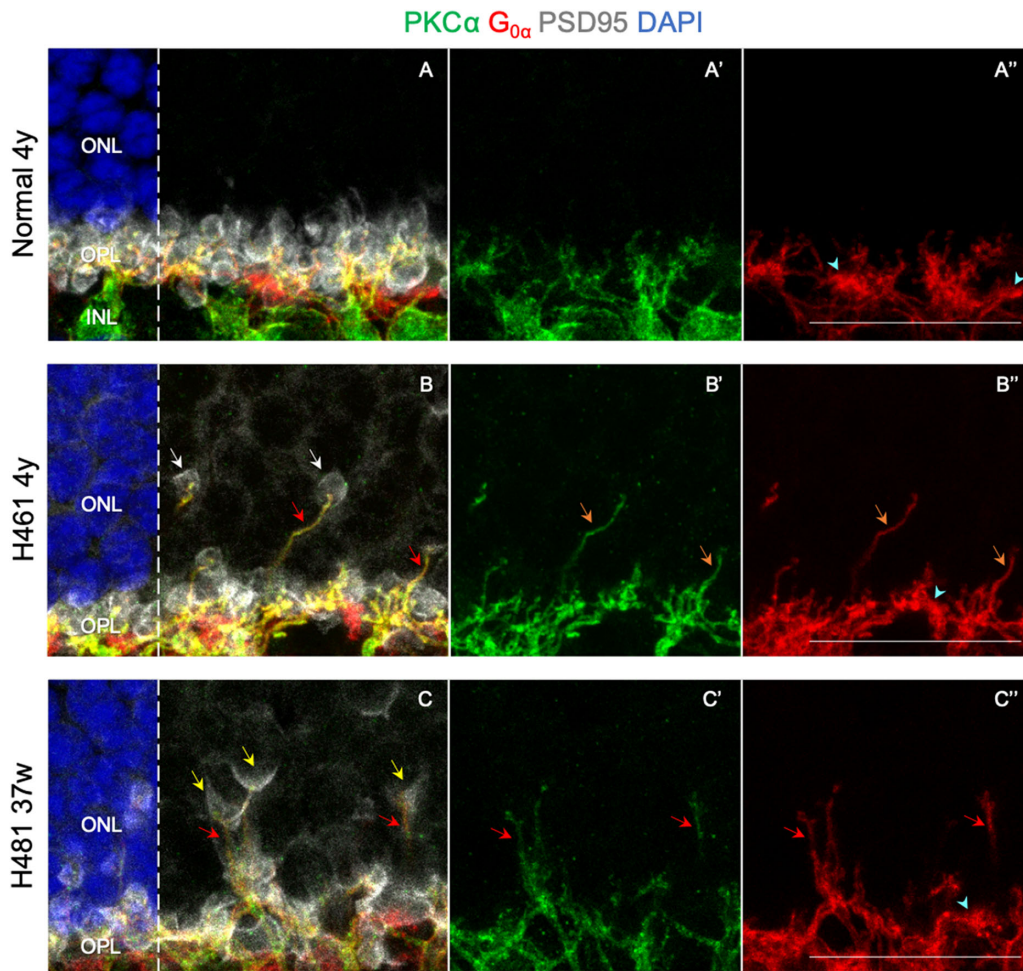


**FIGURE 1.** Sprouting of RBC in XLPRA1. Representative confocal imaging of canine normal (A–A'') and XLPRA-affected retinas (B–B'' and C–C'') immunostained with ON RBC marker PKC $\alpha$  (green), ON cone/rod BC marker G $_{0\alpha}$  (red) and PR terminal marker PSD95 (silver). In normal retina (A–A'') both PR synapses and dendritic fibers of ON BCs are restricted to the OPL. In XLPRA1 retinas (4 years old, B–B'' and 37 weeks, C–C'') retraction of PR terminals (white and yellow arrows) often take place occupying ONL with bipolar cell dendritic processes (red and orange arrows) extending into the ONL. PSD95 labeling shows spherules with partially retracted axons (B, white arrow) as well as fully retracted axon-less PR (C, yellow arrow). The presence of solely yellow (green and red co-labeling) fibers demonstrates that only dendrites of RBC (PKC $\alpha^+$ /G $_{0\alpha}^+$ , red arrow), and not cone bipolar cells (PKC $\alpha^-$ /G $_{0\alpha}^+$ , cyan arrowhead) sprout and appose to both partially retracted and axon-less terminals. INL, inner nuclear layer. For each figure, part of the image is presented as an individual color layer separated by solid line to better illustrate a particular feature. A, B, and C show the merged image for the three channels, including DAPI on the left of each set, separated by dashed line. The images A and C were taken in the midperipheral area of the retina, whereas B was taken in central area. Scale bar = 20  $\mu$ m.

than 0.05 and fold changes of more than  $\pm 2$  were considered differentially expressed.

### Absolute Quantification of Gene Expression

The SYBR green platform was used to determine specific transcript levels in retinal samples using a primer concentration of 0.15  $\mu$ M. Primer sequences are listed in Supplementary Table S2. Specific RT-PCR product was used for construction of an absolute standard curve for individual amplicons representing the characterized sequence. Dilution series of these RT-PCR products ranging from  $10^3$  to  $10^7$  molecules were used to construct standard curves. The number of copies of a template was calculated as described elsewhere.<sup>33</sup> The reaction data were analyzed using the 7500 Software version 2.0.1 (Applied Biosystems).

### Fluorescent Immunohistochemistry

The procedure was carried out as previously described.<sup>18</sup> Briefly, 10- $\mu$ m retinal cryosections were washed and treated with primary antibodies in PBS solution, 3% normal horse serum, 1% BSA, and 0.3% Triton X-100 overnight followed by incubation with appropriate fluorescent secondary antibodies (Alexa Fluor Dyes, 1:200; Molecular Probes, Eugene, OR). Primary antibodies information is provided in Supplementary Table S3 and Supplementary Fig. S1. Labeling was examined by epifluorescence microscopy with a Zeiss Axioplan microscope (Carl Zeiss Meditech, Oberkochen, Germany). Images were digitally captured (Spot 4.0 camera; Diagnostic Instruments, Inc., Sterling Heights, MI) under identical conditions and imported into ImageJ software (National Institutes of Health).<sup>34</sup> Confocal images were captured with TCS-SP5 confocal microscope system (Leica

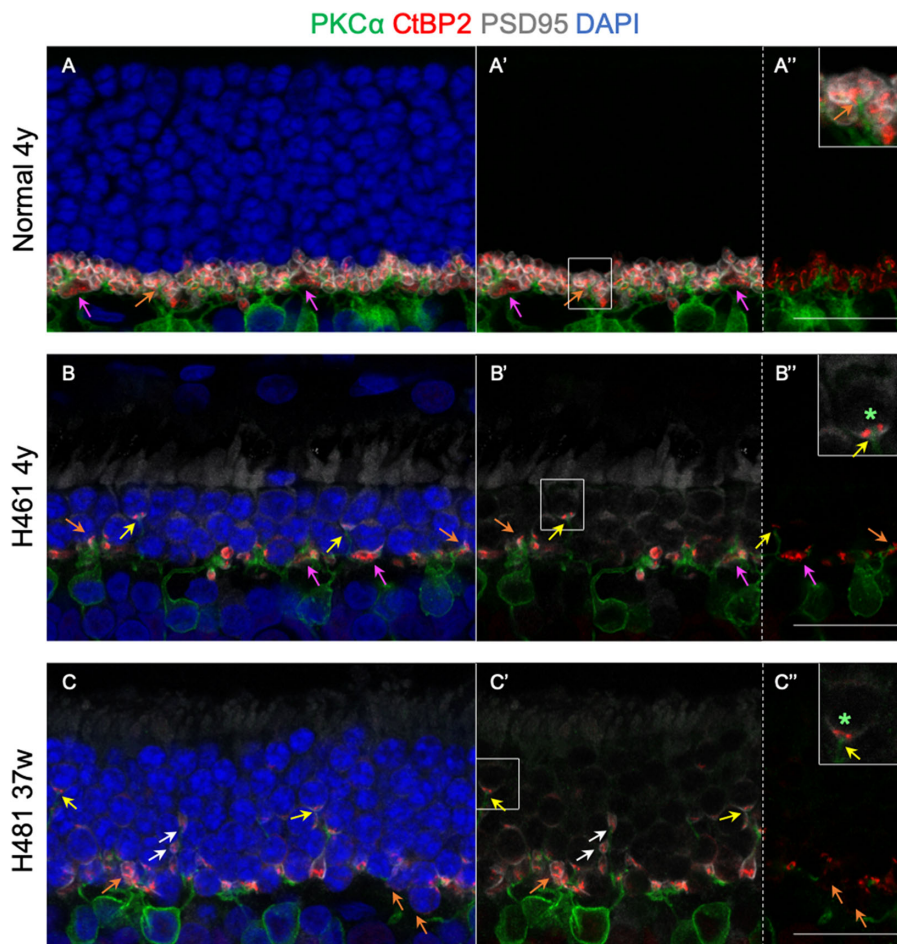


**FIGURE 2.** Synaptic ribbon in retracted axon appose sprouting RBC. Representative confocal imaging of canine normal (**A–A'**) and XLPRA-affected retinas (**B–B'** and **C–C'**) immunolabeled with ON RBC marker PKC $\alpha$  (green), retinal ribbon marker CtBP2 (red) and PR terminal marker PSD95 (silver). In normal retina (**A–A'**), ribbons labeled by CtBP2 staining indicates the location of synaptic contact in PR synaptic terminals couple with PSD95 labeling (**A'**, insert). In disease (**B–B'** and **C–C'**) PSD95 delineates nonretracted (orange arrow) and retracted terminals (partially [*white arrow*], fully [*yellow arrow*]). In fully retracted axons, an apparent higher density of PSD95 coincides with the presence of CtBP2<sup>+</sup> ribbon, suggesting a polarity of molecular signals that pinpoint the position of the synaptic structure in the absence of an axon (*green asterisk*). Ribbon-containing synaptic terminals, including retracted ones, are invaginated by PKC $\alpha$ <sup>+</sup> RBP dendrites. Insert represents a magnified section of the main image and is shown at the corner of each panel. For each figure, a color layer of part of the image (separated by a *dashed line*) is omitted to better illustrate a particular feature. Cone pedicles are indicated by *magenta arrows*. **A**, **B** and **C** show the merged image for all channels. Scale bar = 20  $\mu$ m.

Microsystems, Buffalo Grove, IL) under identical conditions and imported into ImageJ software. Confocal images are shown as a z-stack of 11 z-steps or as a single z-step each of 0.21  $\mu$ m. Maximum projection of all images were equally adjusted for contrast and brightness with ImageJ software. Although the entire retinal expanse was examined in the immunolabeled sections, the images used in the illustrations were taken in midperipheral area of the retina (approximately 6000  $\mu$ m central to the ora serrata [default] unless a different area is specified in the legend to the Figure).

### Western Blot Analysis

Western blots were carried out as previously described<sup>18</sup> using primary antibodies listed in Supplementary Table S3. Protein concentrations were determined by BCA Protein Assay (Thermo Fisher Scientific), and equal micrograms

of protein analyzed. Normalization to ACTB and analyses were performed using Image Studio Software provided by LI-COR BioSciences (Lincoln, NE). Quantification of proteins on western blot was carried out with Li-COR Odyssey software. Western blotting was done in total retinal protein extracts in 16-weeks-old normal and XLPRA1 retinas.

### Sequence Analysis Tools

Protein-conserved domains were characterized using the National Center for Biotechnology Information software BLAST (<https://blast.ncbi.nlm.nih.gov/Blast.cgi?PAGE=Proteins>). Signal peptide and nuclear localization signal (NLS) were predicted with Phobius (<http://phobius.sbc.su.se/>) and cNLS Mapper (<http://nls-mapper.iab.keio.ac.jp/cg/>), respectively.

## RESULTS

## Synaptic Communication Between Rod PRs and Second-Order Neurons in XLPRA1

We first examined the structural changes associated with both the PR synaptic terminals and the processes by which second-order retinal neurons (bipolar and HCs) might evoke dendritic sprouting into the ONL owing to altered synaptic connection. For this purpose, different cellular markers were used to label populations of bipolar, horizontal, and PR cells in the normal and mutant retinas. All ON bipolar cells (RBCs and cone bipolar cells) were stained with antiguanine nucleotide-binding protein G(o) subunit alpha ( $G\alpha$ ), ON-RBCs were labeled with anti-PKC $\alpha$ , HCs were labeled with anti-Parvalbumin (PARV) and PR terminals were labeled with an antibody directed against postsynaptic density protein 95 (PSD95), which labels both cone pedicles and rod spherules<sup>35</sup> and C-terminal-binding protein 2 (CtBP2/RIBEYE; a component of PR ribbons<sup>36</sup>).

Representative images of retinal sections from a 4-year-old normal dog and 37 weeks and 4-year-old XLPRA1-affected dogs labeled with PKC $\alpha$ ,  $G\alpha$ , and PSD95 antibodies show that, in normal adult retina, bipolar cell dendrites and labeled presynaptic sites were confined to the outer plexiform layer (OPL) (Fig. 1A). In the mutant retinas, a number of rod PR synapses retract into the ONL accompanied by the aberrant outgrowth of RBCs dendrites into the ONL (Figs. 1B–C). Furthermore, the sprouted RBC dendrites invaginated into the retracted presynaptic sites, suggesting the potential presence of functional synapses. This possibility was further supported by triple immunolabeling where the tips of RBCs stained with PKC $\alpha$  antibodies are seen in direct apposition to the presynaptic CtBP2 and PSD95 labeling in both normal and XLPRA1 retinas (Fig. 2).

Likewise, processes of HCs labeled with anti-PARV, can be seen to extend well into the ONL in XLPRA1 retinas, coming into contact with retracted rod terminals (Fig. 3). Moreover, when the presynaptic marker PSD95 was used in combination with the postsynaptic markers PKC $\alpha$  and PARV, the labeled presynaptic sites were in close proximity to sprouted dendritic processes of both, RBCs and HCs (Figs. 3B–D), further supporting the potential for functional synaptic connectivity.

As seen in Figures 1–3, there is a heterogeneous population of retracted rod spherules, including spherules connected to their soma by an axon, albeit truncated in length, and axonless synaptic structures connected to their soma directly (represented schematically in Supplementary Fig. S2). Notably, all retracted rod spherules were found to be closely juxtaposed with sprouted dendritic processes of RBCs and HCs. No sprouted dendritic processes of either RBCs or HCs were encountered without connection to the presynaptic sites.

Together these results reveal synaptic remodeling in the outer retina of mutant dogs, including rod PR axon retraction as well as disrupted stratification of RBC and HC neurites. Cone PR and CRB remain seemingly unaffected, because no retracted cone pedicles or sprouted cone bipolar cell dendrites were found in the mutant retinas. Also, our results show that the extent of retinal remodeling observed in XLPRA1 retinas is not strictly age dependent, but rather depends on the severity of retinal cell dysfunction, in agreement with previous studies where we reported a significant variation in the time of onset and the rate of XLPRA1 progression.<sup>14,18</sup>

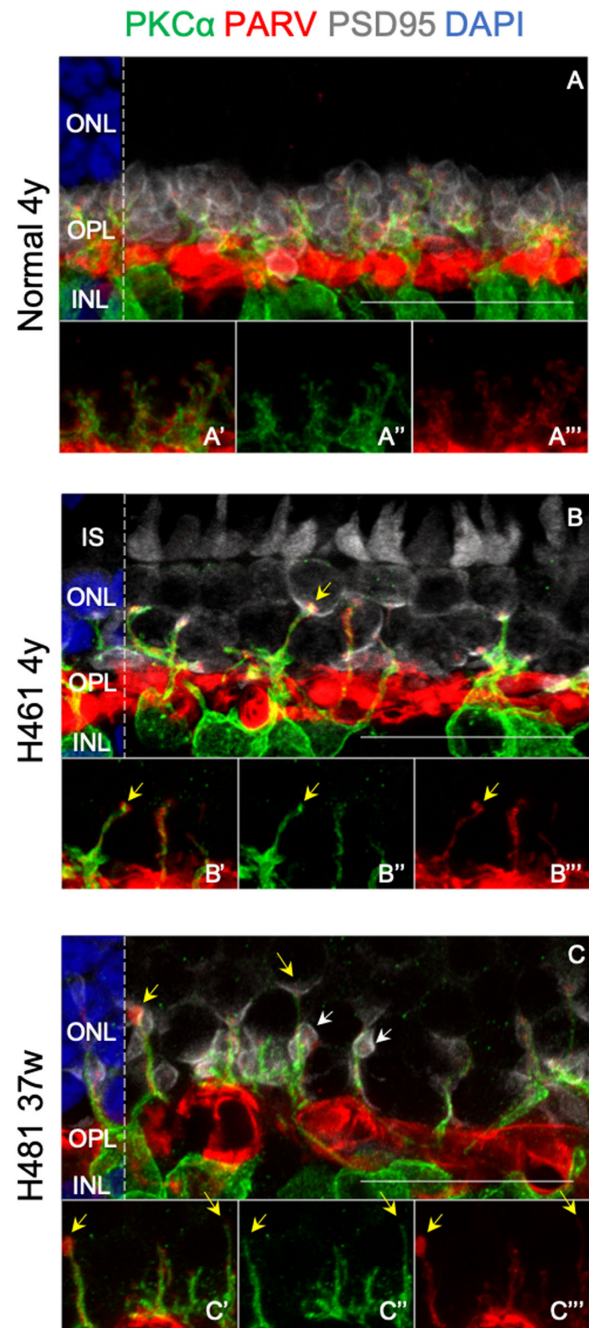


**FIGURE 3.** Retracted axon terminals are invaginated by both RBC and HC. (A–C) Representative confocal imaging of normal canine (A–A''') and XLPRA-affected retinas (B–B''' and C–C''') immunolabeled with ON RBC marker PKC $\alpha$  (green), HC marker PARV (red), and PR terminal marker PSD95 (silver). Nonretracted and retracted (partially [C, white arrow] as well as fully [B–C, yellow arrow]) rod PR terminals, delineated by PSD95 labeling, are invaginated by both RBP and HC sprouting processes. PSD95<sup>+</sup> spherules without invagination by either type of second order neuron processes were not found. For each figure part of the image (separated by a solid line) is presented by combination or an individual color layer to better illustrate a particular feature. The merged image for all channels is on the left of each set (separated by a dashed line). Scale bar = 20  $\mu$ m.

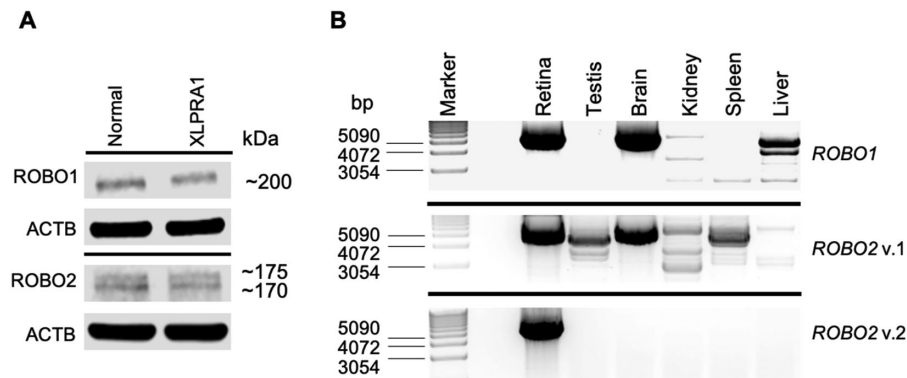


**FIGURE 4.** Expression profiling of canine ROBO1 and ROBO2. **(A)** Western blot analysis of ROBO1 and ROBO 2 proteins in normal and XLPRA1 retinas, 16 weeks old. **(B)** Expression analysis of the ROBO1 and ROBO2 (v.1 and v.2) full-length ORF in different tissues from normal adult dogs.

**TABLE.** Relative and Absolute Quantification of ROBO Transcripts in Normal Canine Retina of Different Ages

Transcript	3 Weeks*	5 Weeks	7 Weeks	16 Weeks
Relative expression				
<i>ROBO2</i> v.1	1	NS	NS	NS
<i>ROBO2</i> v.2	1	NS	NS	NS
<i>ROBO1</i>	1	NS	NS	NS
Absolute expression (copy number $\pm$ SD)				
<i>ROBO2</i> v.1	15,711 $\pm$ 752	5313 $\pm$ 341	9767 $\pm$ 745	9817 $\pm$ 302
<i>ROBO2</i> v.2	15,713 $\pm$ 381	5443 $\pm$ 361	7323 $\pm$ 755	11,252 $\pm$ 877
<i>ROBO1</i>	4379 $\pm$ 299	1718 $\pm$ 52	2703 $\pm$ 123	2676 $\pm$ 130
Absolute expression (approximate ratio between transcripts)				
<i>ROBO2</i> v.1	1	1	1	1
<i>ROBO2</i> v.2	1	1	1	1
<i>ROBO1</i>	0.3	0.3	0.3	0.3

NS, not statistically significant differences.

\*Three weeks is the reference time point.

### Structural and Expression Analysis of the Axon Guidance Receptors ROBO1 and ROBO2

To assess a possible association between an impairment in the ROBO pathway and the synaptic remodeling of rod PRs observed in XLPRA1 retinas, we first examined gene and protein expression of axon guidance receptors ROBO1 and ROBO2, previously uncharacterized in the dog.

The preliminary exon-intron organization of *ROBO1* and *ROBO2* transcripts in canine retina was assembled through alignment of orthologous (human, mice, and bovine) *ROBO1* and *ROBO2* mRNA sequences with the canine genomic sequence and was subsequently validated with RT-PCR. We used 5'RACE was used to analyze the 5' parts of the sequences. Canine *ROBO1* and *ROBO2* genes are located on CFA31 in a tail-to-tail orientation. *ROBO1* encompasses 31 exons (30 coding exons) and has an open reading frame of 4953 nucleotides long that encodes a predicted protein product of 1651 amino acids. Two transcriptional variants of *ROBO2* (v.1 and v.2) driven by alternative promoters separated by 0.67 Mb were also identified in canine retina. Both isoforms were composed of 27 coding exons differing only in their first coding exon. *ROBO2* v.1 open reading frame is 4146 nucleotides long and encodes a predicted protein of 1382 amino acids, whereas the *ROBO2* v.2 open read-

ing frame is 4215 nucleotides long and encodes a protein of 1405 amino acids. Protein-conserved domains and other canine ROBO1 and ROBO2 protein features are defined in Supplementary Table S4. Western blot analysis in normal and XLPRA1 retinas showed the presence of an approximately 200-kDa protein band and an approximately 170/175-kDa doublet band recognized by ROBO1 and ROBO2 antibodies, respectively (Fig. 4A). We found no decrease in ROBO1 protein level in predisease 16-weeks-old XLPRA1 retinas; older samples were not available for Western blot analysis.

We next characterized the tissue specificity and expression levels of *ROBO1* and *ROBO2* transcripts (Fig. 4B). The length of the transcript in retina was considered the reference sequence and any other sized PCR products, likely representing alternative splice variants, were disregarded for the purposes of this study. Based on the length estimation and specificity of PCR primers, we found expression of *ROBO1* in brain and liver, in addition to retina. The band corresponding to *ROBO2* v.1 was detected in testis, brain, and spleen, whereas *ROBO2* v.2 was retina specific. To explore how gene expression of *ROBO1*, *ROBO2* v.1, and *ROBO2* v.2 changes with retinal development, we examined transcript levels in normal retinas of different ages (premature: 3, 5, and 7 weeks; and fully developed: 16 weeks) (Table).

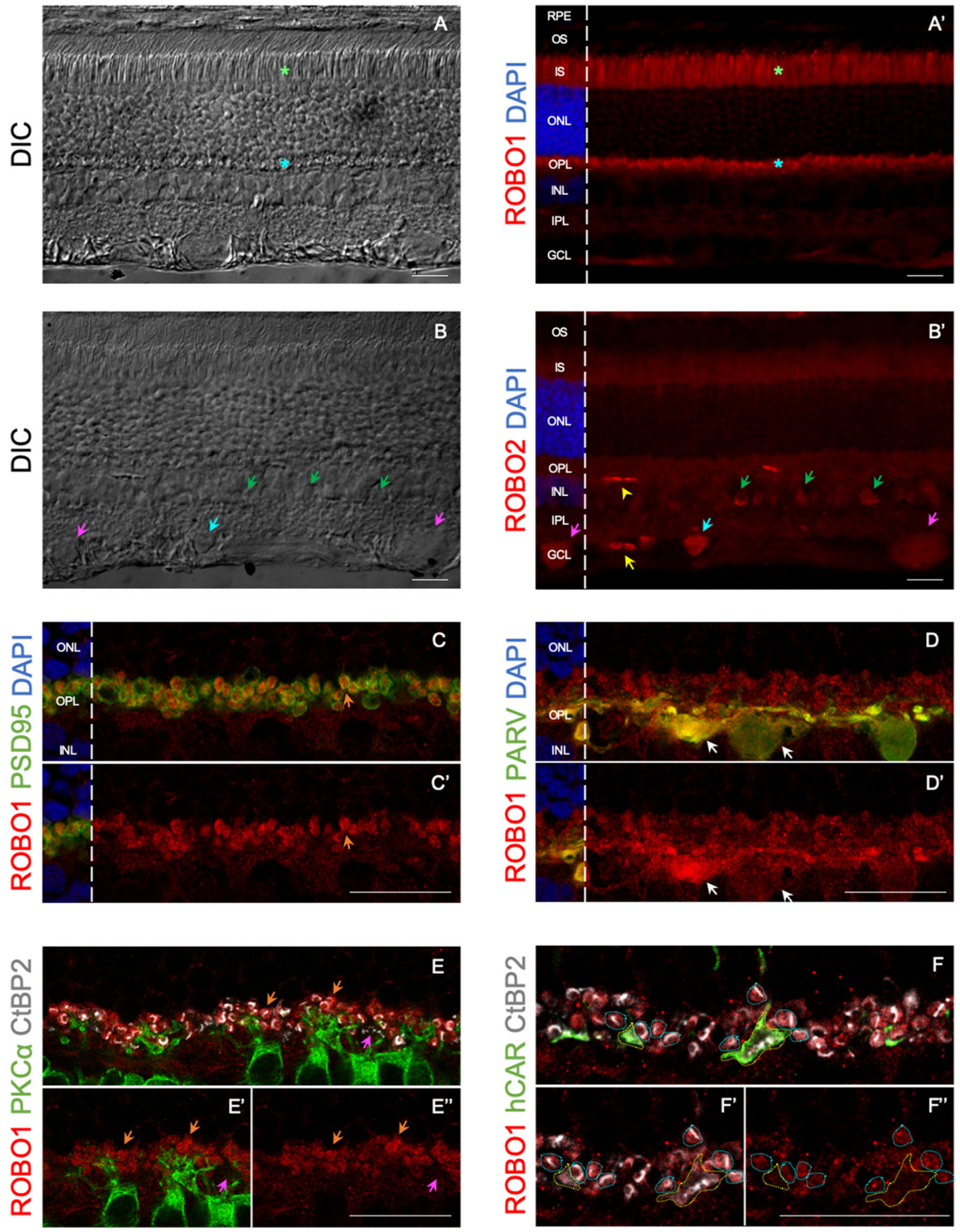


**FIGURE 5.** Expression pattern of ROBOs in normal canine retinas. Immunolabeling of ROBO1 (red), ROBO2 (red), PSD95 (green), CtBP2 (silver), PARV (green), PKCα (green), and cone PR marker hCAR (green) in fully developed normal canine retina (4 years old). (A, B) DIC images for retinal sections on A' and B'. (A') Robust ROBO1 immunolabeling is evident in PR inner segment (green asterisk) and OPL (cyan asterisk). (B') Epifluorescence imaging of ROBO2 staining is prominent in amacrine cell bodies (B', green arrow), displaced amacrine cells (B', cyan arrow) and ganglion cell bodies (B', magenta arrow). Autofluorescence of blood vessels (yellow arrowhead) and erythrocytes (yellow arrow) is noticeable. (C–F'') Confocal imaging shows prominent ROBO1 labeling in rod PR terminals as outlined by PSD95 (C–C', orange arrow) and CtBP2 (E–E'', orange arrow; F–F'', cyan dashed outline). Cone pedicles display negligible labeling of ROBO1 (E, magenta arrow; F, yellow dashed outline). In addition, ROBO1 labeling shows expression in HC as demarcated by PVALB (D–D', white arrow). Where appropriate, a color layer in part of the image (separated by a solid line) is omitted to better illustrate a particular feature. Confocal images (C–F'') are a single z-step image of 0.21 μm. Scale bar = 20 μm.

Results showed stable expression levels of the *ROBO* transcripts in dog retina throughout retinal development, suggesting an important role for these genes in retinal

function. Furthermore, we examined protein expression patterns of ROBO1 and ROBO2 in normal adult retinas. Robust ROBO1 expression is seen in PR inner segment

and OPL (Fig. 5A'). Immunolabeling with ROBO2 antibodies showed detectable expression of this protein in the inner nuclear layer and ganglion cell layer (Fig. 5B'), where ROBO2 displays immunoreactivity to cells labeled with the amacrine cell marker paired box 6 (PAX6)<sup>37</sup> and the ganglion cell marker POU class 4 homeobox 1 (POU4F1/BRN3A)<sup>38</sup> (Supplementary Fig. S3). These data indicate specificity in the expression pattern of ROBO1 versus ROBO2 in adult dog retina with prominent expression of ROBO1 at the site where PR cells form synapses with HCs and bipolar cells.

To detail this finding, we performed immunohistochemistry for ROBO1 and presynaptic or postsynaptic retinal markers. Briefly, strong ROBO1 immunolabeling in normal retina was detected in PR terminals defined by PSD95 (Fig. 5C) and CtBP2 (Figs. 5E-F) staining. Interestingly, confocal imaging showed especially strong ROBO1 labeling in rod spherules (Figs. 5C-F), contrasting with low ROBO1 signal in cone pedicles (Fig. 5F). ROBO1 expression in OPL postsynaptic sites was examined using PARV and PKC $\alpha$  antibodies. In normal retina, ROBO1 labeling is present in PARV<sup>+</sup> (horizontal) cells (Fig. 5D), albeit in lesser amounts than in rod synaptic terminals. We found no evidence of ROBO1 expression in PKC $\alpha$ <sup>+</sup> dendrites (Fig. 5E).

We next sought to determine whether ROBO1 levels in rod terminals varied between normal retinas. Toward this end, we performed triple staining for ROBO1, CtBP2, and PKC $\alpha$  (Supplementary Fig. S4). Despite insignificant variation of ROBO1 levels between samples, we found that ROBO1 labeling was well-preserved in rod spherules in all normal retinas examined. Most significantly, no abnormal neuronal remodeling in outer retina was noted.

Finally, to confirm that expression of ROBO1 protein in retinal OPL is conserved between species we examined the expression of orthologous ROBO1 in human, nonhuman primate, mouse and rat retinas (Supplementary Fig. S5). Similar to dog, ROBO1 labeling was found in the OPL of all species studied, where the protein was present in PR terminals defined by CtBP2 staining.

### ROBO1 Expression in Presynaptic Sites is Decreased in XLPRA1 Retinas

We previously showed that the entire retina in XLPRA1 is affected by the disease process, but is least severe near the optic nerve and progresses in severity centripetally from the periphery.<sup>14</sup> We took advantage of the spatial pattern of PR degeneration present in mutant retinas, to compare the expression level of ROBO1 in presynaptic sites in the midperipheral area of the retina (more affected by disease) and more central (less severe, closer to the optic nerve). Double immunolabeling with ROBO1 and PSD95 antibodies in representative 23-week-old (predisease) and 37-week-old (early disease) retinas shows that ROBO1 levels in rod spherules is markedly decrease in the midperipheral region compared with the control retinas (Fig. 6). Notably, a number of rod PRs with retracted axon terminals were found in the midperipheral area in 37-week-old XLPRA1 retinas, but not in 23-week-old XLPRA1 retina (Figs. 6C, E, G). In contrast, the vast majority of all labeled presynaptic sites were confined to the OPL in the area closer to the optic nerve in mutant retinas examined, although ROBO1 labeling was equally low to the matched midperipheral area

(Figs. 6D, F, H). The results suggest that a decrease in ROBO1 levels in rod spherules precedes rod axon retraction, pointing to a link between reduction of ROBO1 in rod synaptic terminals and subsequent axon retraction.

### DISCUSSION

Retinal remodeling, such as PR axon retraction and/or sprouting of neuronal processes is a well-documented process in human patients with RP as well as in animal models of RP.<sup>2,3,17,20</sup> Such remodeling events are not unique for RP, because they have also been reported in other genetic<sup>3</sup> and environmental diseases such as AMD<sup>22</sup> and the aging retina,<sup>39</sup> as well as retinal detachment.<sup>21,23</sup> However, there is a considerable heterogeneity in the progression of neuronal morphologic changes and network rewiring in retinal dystrophies, owing to the diverse molecular pathways underlying the retinal cell dysfunction. In this study, we examined the disease-associated remodeling of axonal and dendritic processes in the outer retina of affected dogs carrying the XLPRA1 mutation in the *RPGR* gene. Results from this study provide new information on the XLPRA1 disease-associated changes in synaptic connectivity between rod PRs and their target cells, RBCs and HCs.

Late-onset XLPRA1 is a progressive rod-cone retinal degeneration.<sup>14,17,18,40</sup> Notably, opsin mislocalization and rod neurite sprouting were detected in XLPRA1 before any discernible PR degeneration.<sup>17</sup> Moreover, initiation of the immune response in XLPRA1 was observed as early as 16 weeks, long before the time when the earliest structural changes and PR degeneration become apparent.<sup>18,19</sup> ERG studies revealed no detectable abnormalities in the rod- and cone-mediated responses in XLPRA1 dogs younger than 6 months of age,<sup>14</sup> pointing toward neuronal plasticity and possible repairing of visual circuits in the early stages of disease.

Examination of neuronal remodeling events in the outer retina of XLPRA1-affected dogs of different age showed numerous retractions of the axon terminals of rod PRs into the ONL. These axonal changes, driven by unknown molecular cues, precede significant loss of rod PRs and are accompanied by sprouting of RBC dendrites and HC processes into the ONL. What accounts for the differences in connectivity between retracted presynaptic and sprouted postsynaptic sites in early disease retinas versus advanced disease retinas remains to be identified. In retinas with advanced disease where there is a prominent loss of PRs, the synaptic remodeling in the outer retina can be explained, at least partially, by a break of synaptic contacts owing to neuronal death followed by rewiring of synaptic connections between rod PRs and their target cells. In contrast, the observed pattern of remodeling in early disease XLPRA1 retinas supports a dynamic, synchronous movement of both the presynaptic and postsynaptic sites to maintain the synaptic connection between rod PRs and their targets. To establish this point definitively, however, will require additional studies.

The actin cytoskeleton has been proposed to regulate PR axon retraction, although relatively little is known about the underlying mechanism. Prior studies showed that activation of RHOA GTPase, a key regulator of the cytoskeleton, and its downstream signaling effectors mediate rod axonal retraction after retinal detachment and injury.<sup>21,23</sup> We hypothesized that disease-associated perturbations in axon guidance signaling pathways, known to regulate the activity of

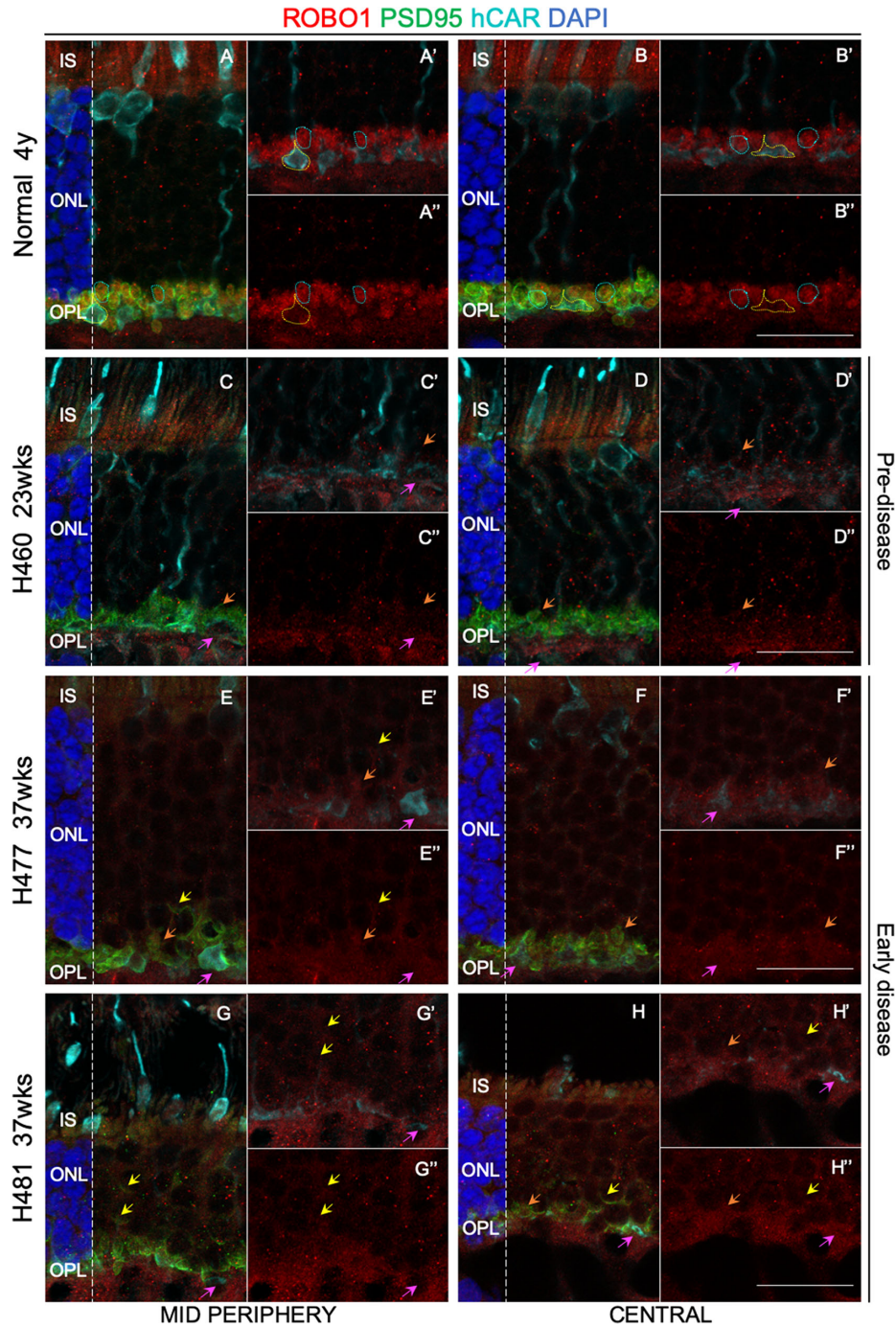


**FIGURE 6.** Expression pattern of ROBO1 in XLPRA1 retinas. Confocal imaging of ROBO1 (red), PSD95 (green), cone PR marker hCAR (cyan) immunolabeling in normal (A–B), predisease (C–D) and early disease (E–H) retinas at midperipheral (approximately 6000 μm from the ora serrata) (A, C, E, G) and central (approximately 10,000 μm from the ora serrata) (B, D, F, H) areas. In normal retina (A–B’), ROBO1 strongly labels rod spherules (cyan outline) and has negligible labeling in cone pedicles (yellow outline). Compared with normal retinas, ROBO1 labeling in XLPRA1-affected retinas is reduced within PR terminals delineated by PSD95 (C–H). Notably, ROBO1 reduction in rod spherules (PSD95<sup>+</sup>/hCAR<sup>-</sup>, C–H’, orange and yellow arrows) in both the midperipheral and central areas in all XLPRA1-affected samples. ROBO1 levels in cone pedicles (PSD95<sup>+</sup>/hCAR<sup>+</sup>, A–H’, magenta arrows) remain seemingly unaffected. In early disease samples, rod axon terminal retraction (PSD95<sup>+</sup>/hCAR<sup>-</sup>) is detected in the midperipheral area (E, G, yellow arrows) but considerably less in the central area (H, yellow arrow). In contrast, the predisease sample does not show axon terminal retraction in either the midperipheral (C, orange arrow) or central areas (D, orange arrow). In both areas examined, ROBO1 labeling in PSD95<sup>+</sup>/hCAR<sup>+</sup> cones is unaffected and pedicles remain confined to the OPL (A–H’, magenta arrow). For each figure part of the image (separated by a solid or dashed line) is presented by omitting a color layer to better illustrate a particular feature. Scale bar = 20 μm.

RHO GTPases, underlie or contribute to rod axon retraction and degeneration. Two evolutionary conserved axon guidance receptors ROBO1 and ROBO2 that mediate repulsion in response to binding of SLIT ligands during neuronal development<sup>25,27,28,41</sup> were tested in this study for possible association between their expression pattern and synaptic remodeling in XLPRA1.

In developing neural tissue, SLIT/ROBO signaling was shown to recruit cytoplasmic kinases and regulatory molecules associated with actin polymerization and microtubule cytoskeleton reorganization,<sup>27,28,42</sup> including the Abelson tyrosine kinase, the enabled protein, and GAPs (Slit-ROBO GTPase-activating protein 1 and RHO GTPase activating protein 39) that inactivate RHO GTPases (RHOA, CDC42), thus modulating cytoskeletal dynamics. Following nervous system development, expression patterns of many axon guidance molecules are decreased, whereas others retain their expression levels and are present in adult neural tissues.<sup>43</sup> Because various mature neurons continue to express receptors for guidance cues, it has been speculated that axon guidance signaling pathways play a role in synaptic stabilization and limitation of neuronal plasticity in adulthood.<sup>43</sup> Expression of ROBO receptors was previously reported in the adult brain, spinal cord, and peripheral nervous system,<sup>44,45</sup> but the presence of ROBO proteins is not limited to neuronal cells. In non-neural tissues, SLIT/ROBO signaling has been linked to roles in angiogenesis, cancer progression, cell migration, and survival among other processes.<sup>27,28,30,46–49</sup> Notably, being expressed in retinal endothelium, ROBO1 and ROBO2 activities promote the migration of endothelial cells and contribute to retinal angiogenesis in health and disease.<sup>30</sup>

In this study, we determined the complete structure and tissue specific expression patterns of one *ROBO1* and two *ROBO2* transcripts that were previously uncharacterized in the dog. Notably, expression of *ROBO1* and *ROBO2* v.1 was found in both retina and brain, whereas expression of *ROBO2* v.2 was limited to the retina. This observation not only supports the importance of the *ROBO* genes in neuronal function, but is also consistent with the possibility that *ROBO* genes are critical for maintaining retinal homeostasis as they exhibit coordinated expression and have a stable ratio between transcripts beginning early in retinal development.

We found that, in fully developed normal retinas, ROBO1 protein is expressed in the inner segment of PRs, and in the OPL, where it is predominantly expressed in rod spherules and to a lesser extent in HC soma/processes. The presence of ROBO1 in rod spherules led us to hypothesize that ROBO1 signaling may be required for presynaptic activity of rod PRs. Moreover, ROBO1 immunolabeling in the inner segment of PRs can reflect both the membrane-localized form and the internalized form of ROBO1 because SLIT-dependent endocytic trafficking of the ROBO1 was shown to be necessary for its signaling output.<sup>50,51</sup> Although it remains to be determined how guidance cues affect the function of PRs, some additional roles for the SLIT/ROBO1 pathway beyond mediating axon responses may be envisioned. One possibility is an involvement of this pathway in regulation of aerobic glycolysis in postmitotic PRs, similarly to reported contribution of SLIT/ROBO1 pathway to the Warburg effect in cancer cells.<sup>52,53</sup>

Furthermore, ROBO2 was found in PAX6<sup>+</sup> and POU4F1<sup>+</sup> retinal neurons, supporting a role for this receptor in amacrine and ganglion cell activities. Notably, these cells

show immunostaining for ROBO2 in both the cell periphery and in the nucleus where ROBO2 displays overlap with neural transcription factors PAX6 and POU4F1 expression patterns (Supplementary Fig. S3). Interestingly, bioinformatics analysis of ROBO2 sequence identified a classical nuclear localization signal at the C-terminus of the protein (Supplementary Table S4), suggesting a possible role of ROBO2 as a regulator of gene expression. If so, this will be in support of the previously proposed hypothesis that signaling from the nucleus may be a common output of axon guidance receptors.<sup>54</sup> Although the presence of ROBO proteins in the nucleus have been previously reported,<sup>48,55</sup> here we present the first observation of nuclear localization of ROBO2 in a subset of retinal neurons.

Next, ROBO1 was selected as a candidate protein to study disease-associated remodeling of PR because it is present in PR synaptic terminals. Analysis of predisease and early disease XLPRA1 retinas identified markedly decreased level of ROBO1 in rod spherules, but no significant changes in ROBO1 levels were noted in cone pedicles and postsynaptic sites. The maintenance of ROBO1 expression in cone pedicles may account for their lack of retraction in this disease. Interestingly, the decrease in ROBO1 levels occurred in XLPRA1 dogs as early as at 23 to 37 weeks when affected retinas are relatively normal morphologically. One cannot exclude the possibility that a critical decrease of ROBO1 levels in rod terminals may trigger actin cytoskeleton rearrangement followed by retraction of rod axon terminals into their cell bodies. These results warrant further investigation.

An important question that remains is what may induce the drop of ROBO1 levels in rod synaptic terminals early in the disease. A defect in intracellular transport and/or processing in ROBO1 levels that might result in mistargeting of the protein in XLPRA1 is a viable hypothesis. Indeed, aberrant protein trafficking is a common feature in retinal degenerative diseases, and for instance the mislocalization of opsin(s) in human and animal models of retinal degeneration have been frequently reported.<sup>12,17,20</sup> Similar to several other *RPGR* disease models,<sup>12,56</sup> opsin mislocalization was detected in XLPRA1 prior to any discernible PR degeneration, although the underlying mechanism(s) is not fully understood.

In conclusion, this study reports remodeling defects in the outer retina of XLPRA1 dogs, including rod PR axon retraction and disrupted stratification of RBC and HC neurites. Moreover, gene and protein expression data suggest a range of functions for the axon guidance receptors ROBO1 and ROBO2 in the retina. Finally, a correlation between reduction of ROBO1 in rod synaptic terminals and subsequent axon retraction appears to be an important early feature of the disease.

### Acknowledgments

The authors thank Noga Vardi, Leslie King, and Jacob Appelbaum for helpful discussions and comments; William Beltran and Svetlana Savina for OCT-embedded retinal tissue; and Gordon Ruthel for assistance in confocal microscopy.

Supported by grants EY06855, EY17549, U24-EY029890, the Foundation Fighting Blindness, the Van Sloun Fund for Canine Genetic Research, Hope for Vision and is partially supported by the Vision Research Center (P30-EY001583). This study used the confocal Microscope in the Penn Vet Imaging Core, which was

purchased with funding from the NIH Shared Instrument Grant S10 OD021633-01.

Disclosure: **T. Appelbaum**, None; **E. Santana**, None; **G.D. Aguirre**, None

## References

- Sahel J, Bonnel S, Mrejen S, Paques M. Retinitis pigmentosa and other dystrophies. *Dev Ophthalmol*. 2010;47:160–167.
- Krishnamoorthy V, Cherukuri P, Poria D, Goel M, Dagar S, Dhingra NK. Retinal remodeling: concerns, emerging remedies and future prospects. *Front Cell Neurosci*. 2016;10:38.
- D'Orazi FD, Suzuki SC, Wong RO. Neuronal remodeling in retinal circuit assembly, disassembly, and reassembly. *Trends Neurosci*. 2014;37:594–603.
- Jones BW, Pfeiffer RL, Ferrell WD, Watt CB, Marmor M, Marc RE. Retinal remodeling in human retinitis pigmentosa. *Exp Eye Res*. 2016;150:149–165.
- Breuer DK, Yashar BM, Filippova E, et al. A comprehensive mutation analysis of RP2 and RPGR in a North American cohort of families with X-linked retinitis pigmentosa. *Am J Hum Genet*. 2002;70:1545–1554.
- Teague PW, Aldred MA, Jay M, et al. Heterogeneity analysis in 40 X-linked retinitis pigmentosa families. *Am J Hum Genet*. 1994;55:105–111.
- Ott J, Bhattacharya S, Chen JD, et al. Localizing multiple X chromosome-linked retinitis pigmentosa loci using multilocus homogeneity tests. *Proc Natl Acad Sci USA*. 1990;87:701–704.
- Vervoort R, Lennon A, Bird AC, et al. Mutational hot spot within a new RPGR exon in X-linked retinitis pigmentosa. *Nat Genet*. 2000;25:462–466.
- Meindl A, Dry K, Herrmann K, et al. A gene (RPGR) with homology to the RCC1 guanine nucleotide exchange factor is mutated in X-linked retinitis pigmentosa (RP3). *Nat Genet*. 1996;13:35–42.
- Wright AF, Shu X. Focus on molecules: RPGR. *Exp Eye Res*. 2007;85:1–2.
- Hong DH, Pawlyk B, Sokolov M, et al. RPGR isoforms in photoreceptor connecting cilia and the transitional zone of motile cilia. *Invest Ophthalmol Vis Sci*. 2003;44:2413–2421.
- Thompson DA, Khan NW, Othman MI, et al. Rd9 is a naturally occurring mouse model of a common form of retinitis pigmentosa caused by mutations in RPGR-ORF15. *PLoS One*. 2012;7:e35865.
- Zhang Q, Acland GM, Wu WX, et al. Different RPGR exon ORF15 mutations in Canids provide insights into photoreceptor cell degeneration. *Hum Mol Genet*. 2002;11:993–1003.
- Zeiss CJ, Acland GM, Aguirre GD. Retinal pathology of canine X-linked progressive retinal atrophy, the locus homologue of RP3. *Invest Ophthalmol Vis Sci*. 1999;40:3292–3304.
- Beltran WA, Hammond P, Acland GM, Aguirre GD. A frameshift mutation in RPGR exon ORF15 causes photoreceptor degeneration and inner retina remodeling in a model of X-linked retinitis pigmentosa. *Invest Ophthalmol Vis Sci*. 2006;47:1669–1681.
- Beltran WA, Cideciyan AV, Lewin AS, et al. Gene therapy rescues photoreceptor blindness in dogs and paves the way for treating human X-linked retinitis pigmentosa. *Proc Natl Acad Sci USA*. 2012;109:2132–2137.
- Beltran WA, Acland GM, Aguirre GD. Age-dependent disease expression determines remodeling of the retinal mosaic in carriers of RPGR exon ORF15 mutations. *Invest Ophthalmol Vis Sci*. 2009;50:3985–3995.
- Appelbaum T, Becker D, Santana E, Aguirre GD. Molecular studies of phenotype variation in canine RPGR-XLPRA1. *Mol Vis*. 2016;22:319–331.
- Appelbaum T, Santana E, Aguirre GD. Strong upregulation of inflammatory genes accompanies photoreceptor demise in canine models of retinal degeneration. *PLoS One*. 2017;12:e0177224.
- Li ZY, Kljavin IJ, Milam AH. Rod photoreceptor neurite sprouting in retinitis pigmentosa. *J Neurosci*. 1995;15:5429–5438.
- Fontainhas AM, Townes-Anderson E. RhoA inactivation prevents photoreceptor axon retraction in an in vitro model of acute retinal detachment. *Invest Ophthalmol Vis Sci*. 2011;52:579–587.
- Sullivan RK, Woldemussie E, Pow DV. Dendritic and synaptic plasticity of neurons in the human age-related macular degeneration retina. *Invest Ophthalmol Vis Sci*. 2007;48:2782–2791.
- Wang W, Halasz E, Townes-Anderson E. Actin dynamics, regulated by RhoA-LIMK-Cofilin signaling, mediates rod photoreceptor axonal retraction after retinal injury. *Invest Ophthalmol Vis Sci*. 2019;60:2274–2285.
- Li S, Mitchell J, Briggs DJ, Young JK, Long SS, Fuerst PG. Morphological diversity of the rod spherule: a study of serially reconstructed electron micrographs. *PLoS One*. 2016;11:e0150024.
- Stoeckli ET. Understanding axon guidance: are we nearly there yet? *Development*. 2018;145(10).
- Bashaw GJ, Klein R. Signaling from axon guidance receptors. *Cold Spring Harb Perspect Biol*. 2010;2:a001941.
- Ypsilanti AR, Zagar Y, Chedotal A. Moving away from the midline: new developments for Slit and Robo. *Development*. 2010;137:1939–1952.
- Blockus H, Chedotal A. Slit-Robo signaling. *Development*. 2016;143:3037–3044.
- Thompson H, Andrews W, Parnavelas JG, Erskine L. Robo2 is required for Slit-mediated intraretinal axon guidance. *Dev Biol*. 2009;335:418–426.
- Rama N, Dubrac A, Mathivet T, et al. Slit2 signaling through Robo1 and Robo2 is required for retinal neovascularization. *Nat Med*. 2015;21:483–491.
- Zhou W, Yu W, Xie W, Huang L, Xu Y, Li X. The role of SLIT-ROBO signaling in proliferative diabetic retinopathy and retinal pigment epithelial cells. *Mol Vis*. 2011;17:1526–1536.
- Zhou W, Wang H, Yu W, et al. The expression of the Slit-Robo signal in the retina of diabetic rats and the vitreous or fibrovascular retinal membranes of patients with proliferative diabetic retinopathy. *PLoS One*. 2017;12:e0185795.
- Kuznetsova T, Zangerl B, Goldstein O, Acland GM, Aguirre GD. Structural organization and expression pattern of the canine RPGRIP1 isoforms in retinal tissue. *Invest Ophthalmol Vis Sci*. 2011;52:2989–2998.
- Schneider CA, Rasband WS, Eliceiri KW. NIH Image to ImageJ: 25 years of image analysis. *Nat Methods*. 2012;9:671–675.
- Koulen P, Fletcher EL, Craven SE, Brecht DS, Wassle H. Immunocytochemical localization of the postsynaptic density protein PSD-95 in the mammalian retina. *J Neurosci*. 1998;18:10136–10149.
- Schmitz F, Konigstorfer A, Sudhof TC. RIBEYE, a component of synaptic ribbons: a protein's journey through evolution provides insight into synaptic ribbon function. *Neuron*. 2000;28:857–872.
- de Melo J, Qiu X, Du G, Cristante L, Eisenstat DD. Dlx1, Dlx2, Pax6, Brn3b, and Chx10 homeobox gene expression defines the retinal ganglion and inner nuclear layers of the

- developing and adult mouse retina. *J Comp Neurol*. 2003;461:187–204.
38. Nadal-Nicolas FM, Jimenez-Lopez M, Sobrado-Calvo P, et al. Brn3a as a marker of retinal ganglion cells: qualitative and quantitative time course studies in naive and optic nerve-injured retinas. *Invest Ophthalmol Vis Sci*. 2009;50:3860–3868.
  39. Liets LC, Eliasieh K, van der List DA, Chalupa LM. Dendrites of rod bipolar cells sprout in normal aging retina. *Proc Natl Acad Sci USA*. 2006;103:12156–12160.
  40. Guyon R, Pearce-Kelling SE, Zeiss CJ, Acland GM, Aguirre GD. Analysis of six candidate genes as potential modifiers of disease expression in canine XLPRA1, a model for human X-linked retinitis pigmentosa 3. *Mol Vis*. 2007;13:1094–1105.
  41. Tong M, Jun T, Nie Y, Hao J, Fan D. The role of the Slit/Robo signaling pathway. *J Cancer*. 2019;10:2694–2705.
  42. Borrell V, Cardenas A, Ciceri G, et al. Slit/Robo signaling modulates the proliferation of central nervous system progenitors. *Neuron*. 2012;76:338–352.
  43. Giger RJ, Hollis ER, 2nd, Tuszynski MH. Guidance molecules in axon regeneration. *Cold Spring Harb Perspect Biol*. 2010;2:a001867.
  44. Carr L, Parkinson DB, Dun XP. Expression patterns of Slit and Robo family members in adult mouse spinal cord and peripheral nervous system. *PLoS One*. 2017;12:e0172736.
  45. Marillat V, Cases O, Nguyen-Ba-Charvet KT, Tessier-Lavigne M, Sotelo C, Chedotal A. Spatiotemporal expression patterns of slit and robo genes in the rat brain. *J Comp Neurol*. 2002;442:130–155.
  46. Brose K, Bland KS, Wang KH, et al. Slit proteins bind Robo receptors and have an evolutionarily conserved role in repulsive axon guidance. *Cell*. 1999;96:795–806.
  47. Ye BQ, Geng ZH, Ma L, Geng JG. Slit2 regulates attractive eosinophil and repulsive neutrophil chemotaxis through differential srGAP1 expression during lung inflammation. *J Immunol*. 2010;185:6294–6305.
  48. Yang YH, Manning Fox JE, Zhang KL, MacDonald PE, Johnson JD. Intraislet SLIT-ROBO signaling is required for beta-cell survival and potentiates insulin secretion. *Proc Natl Acad Sci USA*. 2013;110:16480–16485.
  49. Marlow R, Strickland P, Lee JS, et al. SLITs suppress tumor growth in vivo by silencing Sdf1/Cxcr4 within breast epithelium. *Cancer Res*. 2008;68:7819–7827.
  50. Chance RK, Bashaw GJ. Slit-dependent endocytic trafficking of the Robo receptor is required for Son of Sevenless recruitment and midline axon repulsion. *PLoS Genet*. 2015;11:e1005402.
  51. Kinoshita-Kawada M, Hasegawa H, Hongu T, et al. A crucial role for Arf6 in the response of commissural axons to Slit. *Development*. 2019;146:10.1242/dev.172106.
  52. Petit L, Ma S, Cipi J, et al. Aerobic glycolysis is essential for normal rod function and controls secondary cone death in retinitis pigmentosa. *Cell Rep*. 2018;23:2629–2642.
  53. Zhao SJ, Shen YF, Li Q, et al. SLIT2/ROBO1 axis contributes to the Warburg effect in osteosarcoma through activation of SRC/ERK/c-MYC/PFKFB2 pathway. *Cell Death Dis*. 2018;9:390-018-0419-y.
  54. Neuhaus-Follini A, Bashaw GJ. The intracellular domain of the Frazzled/DCC receptor is a transcription factor required for commissural axon guidance. *Neuron*. 2015;87:751–763.
  55. Seki M, Watanabe A, Enomoto S, et al. Human ROBO1 is cleaved by metalloproteinases and gamma-secretase and migrates to the nucleus in cancer cells. *FEBS Lett*. 2010;584:2909–2915.
  56. Hong DH, Pawlyk BS, Shang J, Sandberg MA, Berson EL, Li T. A retinitis pigmentosa GTPase regulator (RPGR)-deficient mouse model for X-linked retinitis pigmentosa (RP3). *Proc Natl Acad Sci USA*. 2000;97:3649–3654.